Structural, electronic, and magnetic properties of iron carbide Fe_7C_3 phases from first-principles theory

C. M. Fang,[1,2,*] M. A. van Huis,[1,2] and H. W. Zandbergen[2]
[1]*Materials Innovation Institute (M2I), 2628 CJ Delft, The Netherlands*
[2]*Kavli Institute of Nanoscience, Delft University of Technology, Lorentzweg 1, 2628 CJ Delft, The Netherlands*
(Received 29 June 2009; revised manuscript received 17 November 2009; published 22 December 2009)

The iron carbide Fe_7C_3 exhibits two types of basic crystal structures, an orthorhombic (*o*-) form and a hexagonal (*h*-) one. First-principles calculations have been performed for the basic Fe_7C_3 forms and for the related θ-Fe_3C cementite phase. Accurate total-energy calculations show that the stability of Fe_7C_3 is comparable to that of θ-Fe_3C. The *o*-Fe_7C_3 phase is more stable than the hexagonal one, in contrast to recent atomistic simulations. Furthermore, the calculations also show a rather low energy for a carbon vacancy in the *o* structure, which implies possible C deficiency in the lattice. Both Fe_7C_3 phases are ferromagnetic metals. Electronic band-structure calculations show that all Fe atoms exhibit high-spin states with the majority of their 3*d* states being almost fully occupied. From an analysis of the structural and energetic properties, the formation of the *o* phase in steel treatment processes and of *h* form in carburization of ferrite is discussed.

DOI: 10.1103/PhysRevB.80.224108 PACS number(s): 75.50.Bb, 61.50.Lt, 71.15.Nc, 64.60.My

I. INTRODUCTION

In the early 1980s, Bauer-Grosse and co-workers investigated the crystallization processes of amorphous $Fe_{75}C_{25}$ alloys that had been prepared by the sputter-deposition technique. Using transmission electron microscopy (TEM), they found that Fe_7C_3 crystallizes first.[1–3] Fe_7C_3 or more generally $(Fe,M)_7C_3$ (M=Cr, Mn, W, etc.) phases are formed in various preparation and thermal treatment processes of alloys and steels. Examples are white cast alloys,[4,5] Cr-containing ferrite steels, and high-speed steels.[6] Fe_7C_3 forms also as nanoparticles by means of high-pressure techniques[7–9] or by carburization of ferrite.[10–13] Audier and co-workers obtained Fe_7C_3 microcrystals by disproportioning CO on Fe at 500 °C.[14] By means of milling of $Fe_{75}C_{25}$ powder mixture, Campbell and co-workers were able to make Fe_7C_3.[15]

Fe_7C_3 phases exhibit attractive electronic and magnetic properties. Tsuzuki and co-workers found that Fe_7C_3 crystals are ferromagnetic with a Curie temperature of about 250 °C.[8] The materials have high values of saturation magnetization and are investigated for application in magnetic recording media.[9,16,17]

The crystal structures of the Fe_7C_3 phases have been intensively investigated experimentally. On the one hand, Herbstein and Snyman determined Fe_7C_3 to be isostructural to Ru_7B_3 and to have a hexagonal lattice.[18,19] On the other hand, an orthorhombic lattice was determined for Fe_7C_3 by Fruchart and co-workers.[20,21] The relationship between the two structures has been a topic of discussion.[2,3,19,22–27] Senczyk analyzed the lattice relationship of the two structures of Fe_7C_3 and concluded that they are strongly related.[22] Kowalski also reported a number of polytypes of Fe_7C_3.[27] These polytypes can be constructed from the two basic structures: the hexagonal lattice and the orthorhombic one.[18–22,27]

There are only a few theoretical papers about the Fe_7C_3 phases. Xie and co-workers investigated the structures and stability of M_7C_3 (M=Cr, Mn, and Fe) by means of an atomistic approach.[28] They concluded that the hexagonal lattice is favored over the orthorhombic one for Fe_7C_3. Sluiter reported a brief overview of formation enthalpies for various transition-metal carbides using first-principles' methods and found that the *o*-Fe_7C_3 phase is preferred to the *h* form.[29] Until now, however, there is no detailed report on the electronic structure and magnetic properties of the Fe_7C_3 phases. In this work, we present extensive first-principles calculations on the phases. Calculations have been performed for Fe_3C cementite as well for the sake of comparison.[30] The relative stability of the two Fe_7C_3 phases is addressed by means of total-energy calculations with high accuracy and the electronic and magnetic properties are characterized. The information obtained here is helpful to understand the formation and stability of the Fe_7C_3 phases and contributes to a complete understanding of the structural, electronic, and magnetic properties that are of interest to industrial applications.[17,19–27]

II. DETAILS OF CALCULATION METHOD

All calculations were carried out using the first-principles' Vienna *ab initio* simulation program (VASP) code[31–33] employing the density-functional theory (DFT) within the projector-augmented wave (PAW) method.[34,35] The generalized gradient approximation (GGA) was employed for the exchange and correlation energy terms,[36] since it proved that the (spin-polarized) GGA approximation describes spin-polarized Fe better than the (spin-polarized) local-density approximation (LDA).[37] The cutoff energy of the wave functions was 500.0 eV. The cutoff energy of the augmentation functions was 644.5 eV. The electronic wave functions were sampled on an $8\times8\times12$ grid with 70 k points, $4\times8\times12$ with 105 k points, and $10\times8\times12$ with 210 k points, in the irreducible Brillouin zone (BZ) of *h*-, *o*-Fe_7C_3, and θ-Fe_3C, respectively, using the Monkhorst and Pack method.[38] The k mesh has a $24\times24\times24$ grid with 364 k points and a $24\times24\times24$ grid with 413 k points, in the irreducible BZ of α-Fe of the conventional body-centered-cubic (bcc) cell and the primitive cell of diamond, respectively. Magnetism of the iron carbides has been calculated for different orderings. The Wigner-Seitz radius is set to be 1.4 Å for Fe and 1.0 Å for C, respectively, for calculations of partial density of states

and local magnetic moments of atoms. Tests of k mesh and cutoff energies showed a good convergence (well within 1 meV/atom).

III. CALCULATION RESULTS AND DISCUSSION

A. Definition of formation enthalpy

The formation enthalpy (ΔH) of an iron carbide (Fe_nC_m) with respect to the pure elemental solids (α phase of Fe and graphite) can be described as

$$\Delta H = H(Fe_nC_m) - [nH(Fe) + mH(C)]. \quad (1)$$

To compare the relative stability of different iron carbides, we use the formation enthalpy per atom (ΔH_f),

$$\Delta H_f = \Delta H/(n+m). \quad (2)$$

At $T=0$ K and $p=0$ Pa, the formation enthalpy is equal to the difference of the calculated energies, i.e., $\Delta H(Fe_nC_m) = \Delta E(Fe_nC_m)$ when the zero-vibration contribution is ignored.

We first performed total-energy calculations using the settings described in Sec. II for the elemental solids, α-Fe, and diamond. α-Fe has a bcc structure. The calculated lattice parameter $a=2.831$ Å and the local moment $M=2.21\mu_B$/Fe which agree well with the experimental values ($a=2.866$ Å and $M=2.12\mu_B$/Fe) (Ref. 39) and with former theoretical values, e.g., as obtained using ultrasoft pseudopotentials ($a=2.836$ Å and $M=2.17\mu_B$/Fe) (Ref. 39) and the all-electron method ($a=2.848$ Å and $M=2.25\mu_B$/Fe).[40] The calculated energy for α-Fe is 8.310 eV/atom.

Elemental carbon exhibits mainly two phases: graphite and diamond. The ground state of carbon is graphite. Experiments have determined that at $T=0$ K and $p=0$ Pa, graphite is about 17 meV per atom more stable than diamond.[29,41] Graphite exhibits a layered structure. The interlayer bonding is largely determined by van der Waals interactions, which cannot be correctly described by conventional DFT methods.[42] In recent years, many efforts have been made to calculate the interlayer interaction of layered compounds, including graphite, using other theoretical methods.[42–45] The diamond phase, though, can be well addressed with the DFT method used in this work.[46] We therefore adopt the following approach. First, the valence electron energy of diamond is calculated, after which the well-established value of 17 meV per atom is subtracted from the diamond's energy in order to find the valence electron energy for graphite. The calculated lattice parameter for diamond is 3.5713 Å, in good agreement with the experimental value[41] (3.5668 Å at 300 K) and former theoretical calculations.[46]

B. Stability of the Fe_7C_3 phases

As mentioned before, Fe_7C_3 has two forms (see Fig. 1). Herbstein and Snyman determined it to be hexagonal and isostructural to Ru_7B_3 with space group $P6_3mc$ (nr. 186).[18,19] The other form has an orthorhombic lattice.[20–22] Table I shows the calculated lattice parameters of the Fe_7C_3 forms, as well as for θ-Fe_3C. Table II shows the calculated coordinates of atoms and local magnetic moments which were obtained from the difference of the integrated densities of states for the spin-up (majority) and spin-down (minority) electrons in the spheres of the atoms.

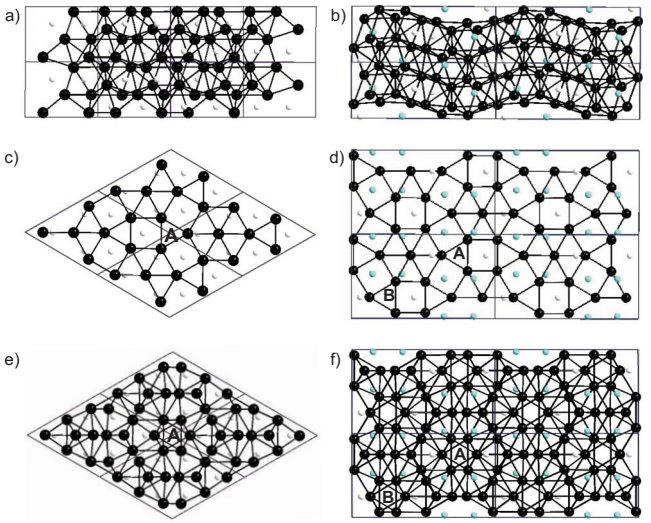

FIG. 1. (Color online) Atomic structure of h-Fe_7C_3 (left-hand side) and o-Fe_7C_3 (right-hand side). (a) Projection of h-Fe_7C_3 along the hexagonal ⟨110⟩ axis and (b) projection of o-Fe_7C_3 along the corresponding orthorhombic ⟨100⟩ axis. [(c)–(f)] Projections of h-Fe_7C_3 and o-Fe_7C_3 along the c axis. (c) and (d) show only one half of the unit cell (along the c axis) so that a single Fe layer in the ⟨001⟩ plane is displayed. (e) and (f) show the projection of the full unit cell so that the octahedrons A (and also B, in the case of the o phase) can be easily identified. The big black and small white (blue) balls represent Fe and C (C2 in the o phase), respectively. Solid lines represent the boundaries of the unit cell.

First we discuss the calculated results of θ-Fe_3C. The calculated lattice parameters are slightly smaller than the reported experimental values (less than 1%, see Table I). Our calculated lattice parameters ($a=5.037$, $b=6.720$, and $c=4.482$ Å) agree well with former theoretical results as well ($a=5.058$, $b=6.703$, and $c=4.506$ Å) by Shein and coworkers using the similar method we use here[47] and ($a=5.079$, $b=6.7137$, and $c=4.5133$ Å) by Faraoun and coworkers using the full-potential linearized augmented plane-wave (FP-LAPW) method.[48] The calculated results for θ-Fe_3C (cementite) and α-Fe can be used as tests of our method and settings.

The calculated lattice parameters for Fe_7C_3 phases are listed in Table I. Our calculations reproduce well the experimental values for the lattice parameters of both hexagonal and orthorhombic cells (within 1%, see Table I). Using the semiempirical atomistic method, Xie and co-workers performed calculations for the Fe_7C_3 phases.[28] Their calculated lattice parameters differ significantly from the experimental data, as shown in Table I. They also reported that the h-Fe_7C_3 is favored over the o form. That disagrees with our calculations. Note that in Table I, for the sake of comparison to the lattice parameters h-Fe_7C_3, we employ the nonstandard space group $Pmcn$ instead of $Pnma$ for o-Fe_7C_3.

It is also noted that the lengths of the a and c axes of the orthorhombic cell are very close to those the hexagonal cell within about 0.5%. The length (11.7324 Å) of the b axis of

TABLE I. Summary of calculated results (lattice parameters, formation enthalpies, etc.). (a) For θ-Fe_3C: orthorhombic with space group *Pnma* (nr. 62). (b) For *h*-Fe_7C_3 with space group *P*63*mc* (nr. 186). (c) For *o*-Fe_7C_3 with space group *Pmcn* (nr. 62).

(a) Lattice	PAW-GGA (present)	PAW-GGA[47]	FP-LAPW-GGA[48]	Exp.[49] (4.2 K)
a (Å)	5.0368	5.058	5.0679	5.082
b (Å)	6.7203	6.703	6.7137	6.733
c (Å)	4.4818	4.506	4.5133	4.514
V (Å^3)	151.71	152.77	153.56	154.40
ΔH_f(meV/at.)	20.6			
(b) Lattice	PAW-GGA (present)	Atomistic[28]	Exp.[18,27]	
a (Å)	6.8243	7.187	6.88	
c (Å)	4.4939	4.235	4.54	
V (Å^3/f.u.)	90.62	94.72	93.05	
ΔH_f(meV/at.)	38.9			
(c) Lattice	PAW-GGA (present)	Atomistic[28]	Exp.[21,27]	
a (Å)	6.8570	6.953	6.879	
b (Å)	11.7324	13.740	11.940	
c (Å)	4.5183	4.991	4.540	
V (Å^3/f.u.)	90.87	119.20	93.22	
ΔH_f(meV/at.)	22.0			

the orthorhombic cell is very close to that of the hexagonal cell ($\sqrt{3}a$=11.8200 Å; here a is the length of a axis of the hexagonal cell).

Next we compare the local structures of the two Fe_7C_3 structures. Figure 1 shows projections of the Fe_7C_3 structures along different directions. As shown in Fig. 1(a), viewed along the ⟨110⟩ axis of *h*-Fe_7C_3, the C atoms are arranged in two parallel lines (z=0.1886 and 0.6886, respectively), while the Fe atoms form two layers along the c axis (centered at z=0 and $\frac{1}{2}$, respectively). Each layer is composed of two Fe sublayers. Figure 1(b) shows the projection of o phase along the ⟨100⟩ axis. The C atoms form two uneven planes, while the Fe atoms form two bulged layers displacing a regular sine curve. Figures 1(c) and 1(d) show the lattices of only one Fe layer for the structures of both the o and h forms, respectively. As shown in Figs. 1(c) and 1(d), the similarity between the two Fe_7C_3 structures is very apparent. In both cases, the Fe atoms form squares and triangles and two-dimensional (2D) hexagonal rings. That agrees with the former discussions about the lattice similarity between the h and o phases.[22–27] Two Fe triangles at closing layers form a prism. There are some differences. One important difference between the two structures is that there is only one type of Fe prisms in the h phase [Fig. 1(e)] while there are two different Fe octahedra in the cell of the o phase [Fig. 1(f)].[22–27] One Fe octahedron is the same as that in the h phase (A type), while the other one is B type formed by turning A octahedron 180° along the c axis.[23,24]

Different possibilities for magnetic ordering of the Fe atoms in the Fe_7C_3 phases were considered. All calculations with different input configurations for magnetic ordering resulted in ferromagnetic ordering for both phases, which is in good agreement with experimental findings.[8]

The calculated lengths of chemical bonds of atoms and the local electronic and magnetic properties are listed in Table II. First we discuss the coordination of carbon atoms in the carbide phases. All the carbon atoms in the Fe_7C_3 phases are coordinated by six Fe atoms, with Fe-C bonds ranging from 1.96 to 2.04 Å, which is similar to the bond lengths in Fe_3C cementite. It is notable that the C2 atoms in the *o*-Fe_7C_3 have an extra Fe-C bond with a slightly longer length of about 2.22 Å, as shown in Table II. Therefore, it is better to describe the C2 atoms being 6+1 coordinated. Meanwhile the C1 atoms have two extra Fe-C bonds with a length of about 2.45 Å. The latter is similar to the carbon atoms in the h form and in the cementite phase (Table II). The Fe atoms in the structures have high Fe coordination numbers (between 11 and 12). In the next section, the atomic arrangements are discussed together with the electronic structure of the compounds.

Table I also includes the calculated formation enthalpies for the two types of Fe_7C_3, as well as for θ-Fe_3C cementite. The calculations show that the *o*-Fe_7C_3 is almost as stable as θ-Fe_3C cementite (formation enthalpies 22.0 and 20.6 meV/atom, respectively). The calculations also show that the orthorhombic lattice has higher stability than the hexagonal one (formation enthalpies 22.0 and 38.9 meV/atom, respectively). In other words, the o phase is about 0.17 eV per Fe_7C_3 more stable than the h phase. This result disagrees with recent atomistic calculations, where the hexagonal phase was predicted to be more stable than the orthorhombic one.[28] Our results are in good agreement, though, with recent first-principles calculations.[29]

TABLE II. Calculated coordinates of atoms, chemical bonds, and local electronic and local magnetic moments: (a) for θ-Fe_3C; (b) for h-Fe_7C_3; (c) for o-Fe_7C_3.

Atom	Site	$x/a, y/b, z/c$	Bonds (Å)	Electronic configuration at Fe 3d	M (μ_B)
(a)					
Fe1	8d	0.1763, 0.0678, 0.3318	-Fe1: 2.45, 2.50, 2.53(×2), 2.62(×2) -Fe2: 2.50, 2.58, 2.63, 2.64, 2.67 -C: 1.99, 2.00, *(2.39)*	4.22↑ 2.30↓	1.88
Fe2	4c	0.0357, $\frac{1}{4}$, 0.8373	-Fe1: 2.50(×2), 2.58(×2), 2.64(×2), 2.64(×2), 2.67(×2) -Fe2: 2.64(×2) -C: 1.96, 1.99	4.26↑ 2.25↓	1.97
C	4c	0.8766, $\frac{1}{4}$, 0.4379	-Fe1: 1.99(×2), 2.00(×2), (2.39(×2)) -Fe2: 1.96, 1.99		−0.14
(b)					
Fe1	2b	1/3, 2/3, 0.4022	-Fe2: 2.51(×3), 2.64(×3), 2.69(×3) -Fe3: 2.62(×3) -C: 1.98(×3)	4.16↑ 2.44↓	1.70
Fe2	6c	0.5456, 0.4544, 0.4089	-Fe1: 2.51, 2.64, 2.69 -Fe2: 2.48(×2), 2.49(×2) -Fe3: 2.61(×2), 2.62(×2) -C: 2.04(×2), (2.44(×2))	4.46↑ 2.05↓	2.03
Fe3	6c	0.1225, 0.8775, 0.5833	-Fe1: 2.62 -Fe2: 2.61(×2), 2.62(×2) -Fe3: 2.51(×2), 2.67(×4) -C: 1.93, 2.00(×2)	4.01↑ 2.51↓	1.46
C	6c	0.1866, 0.8134, 0.1886	-Fe1: 1.98 -Fe2: 2.04(×2), (2.44(×2)) -Fe3: 1.93, 2.00(×2)		−0.12
(c)					
Fe1	4c	1/4, 0.6276, 0.0809	-Fe3: 2.67 -Fe4: 2.48(×2), 2.63(×2), 2.77(×2) -Fe5: 2.57(×2), 2.65(×2) -C1: 1.92 -C2: 1.98(×2)	4.06↑ 2.55↓	1.49
Fe2	4c	1/4, 0.1988, 0.2927	-Fe2: 2.56(×2) -Fe3: 2.51,2.53, 2.69 -Fe4: 2.59(×2), 2.69(×2) -Fe5: 2.50(×2) -C2: 1.99(×2)	4.18↑ 2.36↓	1.79

C. Electronic structure and magnetic properties of Fe_7C_3 phases

The partial and total density of states (DOS) for the two Fe_7C_3 phases and θ-Fe_3C cementite are shown in Fig. 2. As shown in Fig. 2(a), the Fe 4s states have their density of states at around −7.5 to −6.5 eV and are mixed with the C 2p state. The Fe 4p states show no specific peaks. As a whole, the valence band is dominated by the Fe 3d states and

TABLE II. (*Continued.*)

Atom	Site	$x/a, y/b, z/c$	Bonds (Å)	Electronic configuration at Fe 3*d*	*M* (μ_B)
Fe3	4*c*	1/4, 0.4124, 0.2720	-Fe1: 2.67 -Fe2: 2.51, 2.53, 2.69 -Fe4: 2.58(×2) -Fe5: 2.49(×2), 2.64(×2), 2.80(×2) -C1: 1.97 -C2: 1.99(×2)	4.16↑ 2.42↓	1.72
Fe4	8*d*	0.0638, 0.8084, 0.0628	-Fe1: 2.48, 2.63, 2.77 -Fe2: 2.59, 2.69 -Fe3: 2.58 -Fe4: 2.55, 2.64(×2) -Fe5: 2.58, 2.66 -C1: 2.03 -C2: 1.97, 2.04	4.15↑ 2.40↓	1.73
Fe5	8*d*	0.0665, 0.0154, 0.2515	-Fe1: 2.57, 2.65 -Fe2: 2.50 -Fe3: 2.49, 2.64, 2.80 -Fe4: 2.58, 2.66 -Fe5: 2.45, 2,48, 2.52 -C1: 2.01 (2.45) -C2: 2.04, 2.22	4.26↑ 2.29↓	1.97
C1	4*c*	1/4, 0.5620, 0.4697	-Fe1: 1.92 -Fe3: 1.97 -Fe4: 2.03(×2) -Fe5: 2.01(×2) [2.45(×2)]		−0.12
C2	8*d*	0.0261, 0.3528, 0.0400	-Fe1: 1.98 -Fe2: 1.99 -Fe3: 1.99 -Fe4: 1.97, 2.04 -Fe5: 2.04, *2.22*		−0.13

there are no significant contributions from Fe 4*s*, 4*p* states. Therefore, in Figs. 2(b) and 2(c), only the partial densities of states of the Fe 3*d* states are presented. Table III summarizes the characteristics of the electronic structures of the Fe_7C_3 phases and θ-Fe_3C. As shown in Fig. 2, the shapes of partial DOS of the Fe atoms in the Fe_7C_3 phases and θ-Fe_3C cementite are very similar. The calculations also show that the number of electrons in the 3*d* states in the Fe spheres are almost the same (about 6.5 electrons) for the Fe_7C_3 phases and θ-Fe_3C phase. This indicates very similar Fe-Fe environments for the atoms (Table II). Below, we discuss into more detail the local electronic and magnetic features of the three phases.

The overall valence bands of the iron carbides phases consist of two separated parts. The semicore C 2*s* states form a rather broad band (about 2.1–3.0 eV) at the lower energy range (around −12.8 eV, Table III). The C 2*s* bandwidth of *h*-Fe_7C_3 is close to that of θ-Fe_3C, while that of *o*-Fe_7C_3 phase has slightly broader C 2*s* bandwidth, as shown in Table II. The shapes of C 2*s* states are almost identical for both spin-up and spin-down electrons (Fig. 2), which is due to the fact that there is no magnetic moment for the C 2*s* states for the three phases. Figure 2 also shows the disperse character of the semicore C 2*s* states. This indicates that although C 2*s* electrons belong to semicore states, they also contribute to valence interactions. A gap is present between the low-energy range (C 2*s* states) and the upper-energy range (C 2*p* and Fe 3*d* states). The C 2*p* states dominate the lower part of the valence band from the bottom (about −7.5 to about −4.3 eV). However, there are also some unoccupied C 2*p* states above the Fermi level as shown in the Fig. 2. This indicates that the iron carbides are not completely ionic, considering the difference of their electronegativities (the Pauling scale, 1.83 for Fe vs. 2.55 for C). For the itinerant spin-polarized Fe 3*d* electrons, we integrate the occupied density of states in the Wigner-Seitz sphere of an atom, so that we can obtain the local magnetic moment in the sphere from the difference of the occupied spin-up (or majority) and spin-down (minority) densities of states. The local magnetic moment in a C sphere is about $-0.12\mu_B$/C, originating from the hybridization between C 2*p* and Fe 3*d* states. There are apparent differences in the shapes of Fe 3*d* density of states as shown in Fig. 2. The corresponding local chemical environments are shown in Table II. For all the iron atoms, the Fermi level is at the top of the Fe 3*d* states for the spin-up electrons as shown in Fig. 2. Therefore, the Fe atoms are

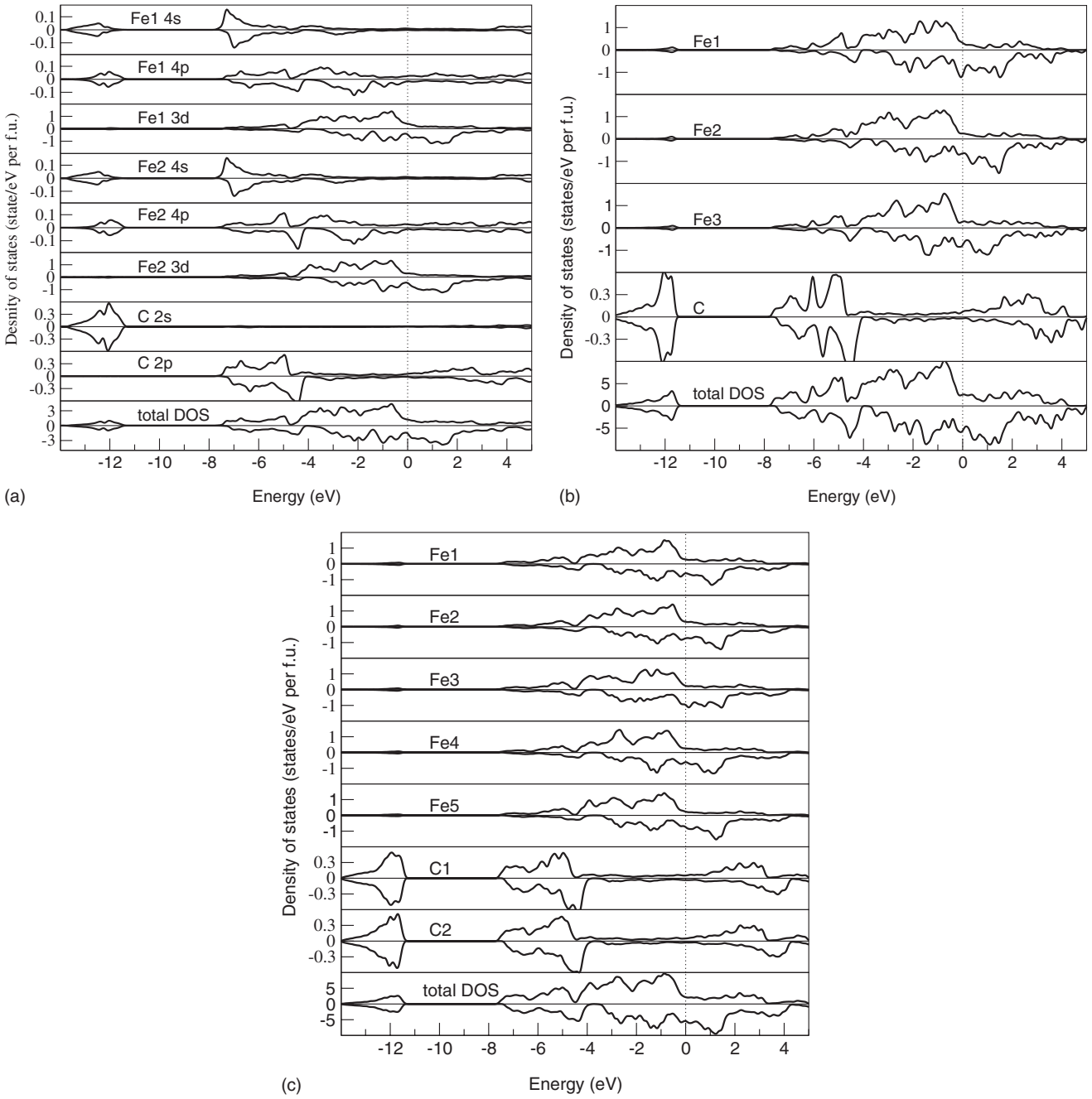

FIG. 2. Partial and total densities of states for θ-Fe_3C, (a) cementite, (b) h-Fe_7C_3, and (c) o-Fe_7C_3. The Fermi level is set to be at 0 eV. The unit for density of states is states/eV per atom for the atoms and states/eV per formula unit for the total density of states (total DOS). The DOSs of C atoms in (b) and (c) include the well-separated $2s$ and $2p$ states.

almost fully spin polarized, in line with electronic structure of α-Fe.[39,50,51]

The local magnetic moments in the Fe spheres show small differences, $1.88\mu_B$ for Fe1 and $1.97\mu_B$ for Fe2 in θ-Fe_3C, as shown in Table II. This corresponds with a similar local chemical bonding, as well a similar local electronic structure (Fig. 2). As shown in Table II, there are Fe atoms having small magnetic moments: $1.46\mu_B$ for Fe3 in the h-Fe_7C_3 and $1.49\mu_B$ for Fe1 in o-Fe_7C_3, originating from the Fe-C bonding. Table II shows that Fe atoms with short Fe-C bonds (about 1.93 Å) have a lower occupation of the spin-up $3d$ states (Fig. 2). Moreover, the Fe2 atom in h-Fe_7C_3 and the Fe5 atom in o-Fe_7C_3 have a local moment of about $2.0\mu_B$. Those types of Fe have long Fe-C bonds (>2.0 Å). These results agree with the general convention that strong Fe-C bonding can reduce the local magnetic moment of Fe atoms.

D. Formation of the Fe_7C_3 phases

The coordination numbers (CNs) for Fe atoms by other Fe atoms for the three structures in Table II are in the range between 11 and 12. These numbers are much larger than that in α-Fe (CN=8), but close to that in γ-Fe (CN=12). This can be understood from the fact that the Fe sublattices of the

TABLE III. Characteristics of the electronic structures of the Fe_7C_3 phases and θ-Fe_3C.

Phase	h-Fe_7C_3	o-Fe_7C_3	θ-Fe_3C	θ-Fe_3C [a]	θ-Fe_3C [b]
Bandwith of C 2s (eV) (range)	2.2	2.6	2.2		~2.3
	(−14.1 to −11.9)	(−14.0 to −11.4)	(−13.7 to −11.5)		~(−13.7 to −11.4)
Bandwith of C 2p (eV) (range)	2.8↑	3.1↑	3.0↑	2.9↑	2.8↑
	(−7.3 to −4.5)↑	(−7.6 to −4.5)↑	(−7.7 to −4.7)↑	(−7.7 to −4.8)↑	(−7.5 to −4.7)↑
	3.5↓	3.5↓	3.4↓	3.2↓	3.3↓
	(−7.5 to −4.0)↓	(−7.3 to −3.9)↓	(−7.5 to −4.1)↓	(−7.4 to −4.2)↓	(−7.4 to −4.1)↓
Bandwith of Fe 3d (eV) (range)	4.6↑	4.4↑	4.5↑	4.5↑	~4.5 ↑
	(−4.6 to 0.0)↑	(−4.4 to 0.0)↑	(−4.5 to 0.0)↑	(−4.5 to 0.0)↑	~(−4.5 to 0.0)↑
	6.0↓	5.6↓	6.3↓	6.0↓	~6.1↓
	(−3.7 to +2.3)↓	(−3.3 to +2.3)↓	(−3.6 to +2.7)↓	(−3.4 to +2.6)↓	~(−3.5 to +2.6)↓
DOS at E_F states/eVFe	0.3↑	0.3↑	0.4↑	~0.4↑	
	0.8↓	0.8↓	0.5↓	~0.5↓	

[a]Reference 47.
[b]Reference 48.

Fe_7C_3 structures, being similar to that of θ-Fe_3C, are basically distorted closed packed structures (Fig. 1). Therefore, the Fe sublattices play a determining role in the structures of Fe_7C_3. In order to analyze this further, the Fe sublattices of the phases have been calculated for several configurations of Wyckoff site occupancies. The influence of magnetic ordering was taken into account as well.

As shown in Table II, there are four kinds of atoms in the h-Fe_7C_3. Fe1 atoms are positioned at 2b, Fe2 and Fe3 at two sets of the 6c sites while C atoms are at 6c. In the lattice, the Wyckoff 2a sites are unoccupied. Therefore, we assumed several possible structural configurations including changes in chemical composition. For o-Fe_7C_3, there are seven kinds of atoms: five types of Fe atoms with three of them at three sets of 4c sites and two of them at two sets of 8d sites. Furthermore, two kinds of carbon atoms are positioned at 4c and 8d sites. Considering the Fe-Fe atomic environment, all the Fe atoms in the o phase are strongly bonded to each other (Table II) and therefore we only consider possible carbon deficiency. Table IV lists the possible changes and arrangements of atoms for the orthorhombic Fe_7C_3 phase.

TABLE IV. Calculated results (lattice parameters, formation enthalpies). FM represents for the ferromagnetic ordering and FR for a ferrimagnetic ordering.

Model	Atoms at Wyckoff sites	Formula/magnetism	Lattice (Å)	ΔE (meV/atom)
Orthorhombic, space group: *Pnma* (nr. 62)				
Model a	Fe: 4c, 4c, 4c, 8d, 8d C: 4c, 8d	Fe_7C_3/FM	a=6.8570 b=11.7324 c=4.5183	22.0
Model b	Fe: 4c, 4c, 4c, 8d, 8d C: 8d	Fe_7C_2	a=6.9491 b=11.7883 c=4.3340	74.8
Model c	Fe: 4c, 4c, 4c, 8d, 8d C: 4c	Fe_7C_1	a=6.8453 b=11.9606 c=4.2168	161.6
Model d	Fe: 4c, 4c, 4c, 8d, 8d	Fe_7C_0	a=7.0824 b=11.8679 c=4.0630	226.0
Hexagonal, space group $P6_3mc$ (186)				
Model 1	Fe: 2b, 6c, 6c C: 6c	Fe_7C_3/FM	a=6.8243 c=4.4939	38.9
Model 2	Fe: 2a, 6c, 6c C: 6c	Fe_7C_3/FR	a=7.1129 c=4.3340	318.2
Model 3	Fe: 6c, 6c C: 6c	Fe_6C_3/FM	a=6.5548 c=4.5332	196.2
Model 4	Fe: 2a, 2b, 6c, 6c C: 6c	Fe_8C_3/FR	a=7.0483 c=4.7513	400.5
Model 5	Fe: 2b, 6c, 6c	Fe_7C_0/FM	a=6.4897 c=4.0691	329.5

Table IV shows that the pure Fe sublattices in o-Fe_7C_3 are more stable than those in the h-Fe_7C_3. Moreover, the o-Fe_7C_2 has a formation enthalpy of just 74.8 meV/atom relative to that of the elemental solids. In other words, the formation of a carbon vacancy has a low energetic cost of 0.45 eV. These results indicate that the o-Fe_7C_3 may exhibit C deficiency. In contrast, the Fe sublattices in the h-Fe_7C_3 structure are less stable than those of o phase and the carbon atoms play a crucial role in the stabilization of the hexagonal structure, particular in nonstoichiometric environments.

Experimental observations revealed that in steels, the o-form phase occurs more frequently than the h phase[30] and that there are a number of polytypes of Fe_7C_3.[27] The formation of polytypes originates from twinning or antiphase ordering of the o structure. On the other hand, h structure (or a pseudohexagonal lattice) was often observed in the crystallization of amorphous alloys[1–3] and carburization of iron.[9–13] It is well known that complex processes such as nucleation and growth of a carbide in amorphous alloys, carburization, and precipitation in steels depend on many factors, such as chemical composition, thermal history, temperature, and interface interactions with the other phases. Our calculations show that the o-Fe_7C_3 has a more stable Fe sublattice and may contain carbon (vacancy) defects. Therefore the stability of o-Fe_7C_3 is not strongly dependent on the carbon content in steels and the nucleation of o-Fe_7C_3 in steels is easier than that of the h form. In general, o-Fe_7C_3 is formed in residual austenite with stacking faults. The cavities of the Fe sublattices in the o phase will then trap carbon atoms from the environment. Moreover, as pointed out by several authors, order and disorder defects cause the polytypism of Fe_7C_3.[27] On the other hand, it has been reported that carburization of ferrite will produce mainly nanosized particles of h-Fe_7C_3 from chemically produced C clusters.[9–13] For the nanocrystals obtained by methods such as carburization of iron, the defects causing the formation of different Fe_7C_3 lattices may not be observed by methods such as x-ray diffraction. Audier and co-workers obtained microcrystals of o-Fe_7C_3 by disproportioning CO on Fe at 500 °C,[14] suggesting that the h phase transformed into the o phase (through stacking fault generation) as the nanoparticles increase in size.

IV. CONCLUSIONS

Total energy and electronic structure calculations were performed for the two basic lattices of Fe_7C_3 and for θ-Fe_3C cementite, the most common carbide in steels. Total energy calculations show that the Fe_7C_3 phases are slightly less stable that θ-Fe_3C, in agreement with experimental observations. Moreover, o-Fe_7C_3 is preferred to the h form at $T=0$ K and $p=0$ Pa, in contrast to recent semiempirical atomistic calculations.[28] Both forms of Fe_7C_3 exhibit ferromagnetic ordering. All the Fe atoms are at a high-spin state. The Fe atoms with a short Fe-C bond (<1.95 Å) have smaller local magnetic moments. The calculations also show that the Fe sublattices in the o-Fe_7C_3 structure exhibit higher stability than the Fe sublattice in the h form. Furthermore, a surprisingly low-energy cost was found for carbon-vacancy formation in o-Fe_7C_3 lattices. The more diverse structure and low carbon-vacancy energy likely enhance the formation of o-Fe_7C_3 in steels.

ACKNOWLEDGMENTS

We appreciate kind help and discussions with M. H. F. Sluiter (Delft University of Technology). D. Hanlon and S. Celotto (Corus RDT) are acknowledged for useful discussion. The authors acknowledge financial support from the Materials Innovation Institute (M2i), Project No. MC5.06280, and from the Stichting Techniek en Wetenschap (STW), Project No. 07532, The Netherlands.

*Corresponding author. FAX: +31 15 2786600; cfang@tudelft.nl

[1] E. Bauer-Grosse, C. Frantz, G. Le Caer, and N. Heiman, J. Non-Cryst. Solids **44**, 277 (1981).
[2] E. Bauer-Grosse, J. P. Morniroli, G. Le Caer, and C. Frantz, Acta Metall. **29**, 1983 (1981).
[3] E. Bauer-Grosse, J. Morniroli, C. Frantz, and G. Le Caer, J. Phys. Colloq. **43**, C9-285 (1982).
[4] A. Inoue and T. Masumoto, Metall. Trans. A **11**, 739 (1980).
[5] S. D. Carpenter and D. Carpenter, Mater. Lett. **57**, 4456 (2003).
[6] I. M. Moustafa, M. A. Moustafa, and A. A. Nofal, Mater. Lett. **42**, 371 (2000).
[7] M. M. Serna, E. R. B. Jesus, E. Galego, L. G. Martinez, H. P. S. Corrêa, and J. L. Rossi, Mater. Sci. Forum **530-531**, 48 (2006).
[8] A. Tsuzuki, S. Sago, S.-I. Hirano, and S. Naka, J. Mater. Sci. **19**, 2513 (1984).
[9] W. Z. Wu, Z. P. Zhu, Z. Y. Liu, Y. N. Xie, J. Zhang, and T. D. Hu, Carbon **41**, 317 (2003).
[10] V. D. Blank, B. A. Kulnitskiy, D. V. Batov, U. Bangert, A. Gutiérrez-Sosa, and A. J. Harvery, Diamond Relat. Mater. **11**, 931 (2002).
[11] X. X. Bi, B. Ganguly, G. P. Huffman, F. E. Huggins, M. Endo, and P. C. Eklund, J. Mater. Res. **8**, 1666 (1993).
[12] C. A. Grimes, D. Qian, E. C. Dickey, J. L. Allen, and P. C. Eklund, J. Appl. Phys. **87**, 5642 (2000).
[13] K. Miura, M. Itoh, and K. Machida, Jpn. J. Appl. Phys. **47**, 2342 (2008).
[14] M. Audier, P. Bowen, and W. Jones, J. Cryst. Growth **63**, 125 (1983).
[15] S. J. Campbell, G. M. Wang, A. Calka, and W. A. Kaczmarek, Mater. Sci. Eng., A **226-228**, 75 (1997).
[16] J. E. Hofer and E. M. Cohn, J. Am. Chem. Soc. **81**, 1576 (1959).
[17] S. Tajima and S.-I. Hirano, Jpn. J. Appl. Phys. **29**, 662 (1990).
[18] F. H. Herbstein and J. A. Snyman, Inorg. Chem. **3**, 894 (1964).
[19] J. M. Morniroli, H. Ayatti, K. M. Knowles, W. M. Stobbs, and M. Gantois, J. Less-Common Met. **155**, 215 (1989).
[20] R. J. P. Fruchart, J. P. Senateur, J. P. Bouchaud, and A. Michel, Bull. Soc. Chim. Fr. **2**, 392 (1965).
[21] R. J. Fruchart and A. Rouault, Ann. Chim. (Paris) **4**, 143 (1969).
[22] D. Senczyk, Phase Transitions **43**, 153 (1993).
[23] S. Nagakura and S. Oketani, Transactions Iron Steel Inst. Jpn. **8**,

265 (1968).
[24] J. P. Morniroli and M. Gantois, J. Appl. Crystallogr. **16**, 1 (1983).
[25] J. Mahy, D. van Dyck, and S. Amelinckx, Philos. Mag. A **50**, 441 (1984).
[26] J. P. Morniroli, M. Khachfi, A. Courtois, M. Gantois, J. Mahy, D. van Dyck, J. van Landuyt, and S. Amelinckx, Philos. Mag. A **56**, 93 (1987).
[27] M. Kowalski, J. Appl. Crystallogr. **18**, 430 (1985).
[28] J.-Y. Xie, N.-X. Chen, J. Shen, L. D. Teng, and S. Seetharaman, Acta Mater. **53**, 2727 (2005).
[29] M. H. F. Sluiter, *Phase Stability of Carbides and Nitrides in Steel*, edited by D. N. Seidman, P. Bellon, C. Abromeit, and J.-L. Boquet, MRS Fall-meeting Boston 2006, session HH(200) Materials Research Society Symposium Proceedings Vol. 979E, (Materials Research Society, Warrendale, PA, 2007).
[30] B. G. Hyde, S. Andersson, M. Bakker, C. M. Plug, and M. O'keeffe, Prog. Solid State Chem. **12**, 273 (1979).
[31] G. Kresse and J. Hafner, Phys. Rev. B **47**, 558 (1993).
[32] G. Kresse and J. Hafner, Phys. Rev. B **49**, 14251 (1994).
[33] G. Kresse and J. Furthmueller, Comput. Mater. Sci. **6**, 15 (1996).
[34] P. E. Blöchl, Phys. Rev. B **50**, 17953 (1994).
[35] G. Kresse and D. Joubert, Phys. Rev. B **59**, 1758 (1999).
[36] J. P. Perdew, K. Burke, and M. Ernzerhof, Phys. Rev. Lett. **77**, 3865 (1996).
[37] C. Amador, W. R. L. Lambrecht, and B. Segall, Phys. Rev. B **46**, 1870 (1992).
[38] H. J. Monkhorst and J. D. Pack, Phys. Rev. B **13**, 5188 (1976).
[39] G. A. de Wijs, G. Kresse, L. Vočadlo, D. Dobson, D. Alfė, M. J. Gillan, and G. D. Price, Nature (London) **392**, 805 (1998).
[40] L. Stixrude, R. E. Cohen, and D. J. Singh, Phys. Rev. B **50**, 6442 (1994).
[41] SGTE Unary Database version v4.4, 20 July 2001. See, e.g., *Thermodynamic Properties of Inorganic Materials*, edited by P. Franke and D. Neuschültz, Landolt-Börnstein, New Series, Group IV: Phys. Chem. Vol 19 XXVI, Scientific Group Thermodata Europe (SGTE) (Springer, Berlin, 2002).
[42] M. Hasegawa, K. Nishidate, and H. Iyetomi, Phys. Rev. B **76**, 115424 (2007).
[43] H. Rydberg, M. Dion, N. Jacobson, E. Schröder, P. Hyldgaard, S. I. Simak, D. C. Langreth, and B. I. Lundqvist, Phys. Rev. Lett. **91**, 126402 (2003).
[44] O. A. Vydrov and T. van Voorhis, J. Chem. Phys. **130**, 104105 (2009).
[45] E. Ziambaras, J. Kleis, E. Schröder, and P. Hyldgaard, Phys. Rev. B **76**, 155425 (2007).
[46] M. Itoh, M. Kotani, H. Naito, T. Sunada, Y. Kawazoe, and T. Adschiri, Phys. Rev. Lett. **102**, 055703 (2009).
[47] I. R. Shein, N. I. Medvedeva, and A. L. Ivanovskii, Physica B **371**, 126 (2006).
[48] H. I. Faraoun, Y. D. Zhang, C. Esling, and H. Aourag, J. Appl. Phys. **99**, 093508 (2006).
[49] I. G. Wood, L. Vočadlo, K. S. Knight, D. P. Dobson, W. G. Marshall, G. D. Price, and J. Brodholt, J. Appl. Crystallogr. **37**, 82 (2004).
[50] C. M. Fang, R. A. de Groot, M. M. J. Bischop, and H. van Kempen, Surf. Sci. **445**, 123 (2000).
[51] T. E. Jones, M. E. Eberhart, and D. P. Clougherty, Phys. Rev. Lett. **100**, 017208 (2008).